Mitochondrial fission promotes radiation-induced increase in intracellular Ca^{2+} level leading to mitotic catastrophe in mouse breast cancer EMT6 cells

Tomoki Bo, Tohru Yamamori, Kumiko Yamamoto, Masaki Fujimoto, Hironobu Yasui, and Osamu Inanami*

Laboratory of Radiation Biology, Department of Applied Veterinary Sciences, Faculty of Veterinary Medicine, Hokkaido University, Sapporo, Japan

*Corresponding author:

Prof. Osamu Inanami

Address: Kita 18, Nishi 9, Kita-ku, Sapporo, Hokkaido 060-0818, Japan

Tel: +81-11-706-5235

Fax: +81-11-706-7373

E-mail: inanami@vetmed.hokudai.ac.jp

Abbreviations: AA-2G, 2-glucopyranoside ascorbic acid; Drp1, dynamin-related protein 1; Fis1, mitochondrial fission protein 1; HCC, human hepatocellular carcinoma; MEFs, mouse embryo fibroblasts; Mfn1/2, mitofusin 1/2; NAC, N-acetylcysteine; Opa1, optic atrophy 1; ROS, reactive oxygen species

ABSTRACT

Mitochondrial dynamics are crucial for cellular survival in response to various stresses. Previously, we reported that Drp1 promoted mitochondrial fission after x-irradiation and its inhibition resulted in reduced cellular radiosensitivity and mitotic catastrophe. However, the mechanisms of radiation-induced mitotic catastrophe related to mitochondrial fission remain unclear. In this study, we investigated the involvement of cellular ATP production, ROS generation, and Ca^{2+} levels in mitotic catastrophe in EMT6 cells. Knockdown of Drp1 and Fis1, which are mitochondrial fission regulators, resulted in elongated mitochondria and significantly attenuated cellular radiosensitivity. Reduced mitochondrial fission mainly decreased mitotic catastrophe rather than necrosis and apoptosis after irradiation. Cellular ATP contents in Drp1 and Fis1 knockdown cells were similar to those in control cells. N-acetylcysteine and 2-glucopyranoside ascorbic acid have no effect on mitotic catastrophe after irradiation. The cellular $[Ca^{2+}]i$ level increased after irradiation, which was completely suppressed by Drp1 and Fis1 inhibition. Furthermore, BAPTA-AM significantly reduced radiation-induced mitotic catastrophe, indicating that cellular Ca^{2+} is a key mediator of mitotic catastrophe induction after irradiation. These results suggest that mitochondrial

fission is associated with radiation-induced mitotic catastrophe via cytosolic Ca^{2+} regulation.

Keywords: Ca^{2+}, Calcium regulation, Fission, Mitochondria, Mitotic catastrophe, Radiation

1. INTRODUCTION

Mitochondria greatly contribute to the cellular quality and function, and mitochondrial function is essential for cell survival. Mitochondria are dynamic organelles that constantly change shape, by a process called mitochondrial dynamics. Mitochondrial dynamics consist of two processes, fission and fusion, and the balance of these processes is important for the regulation of mitochondrial function [1]. Mitochondrial fission and fusion are regulated by several proteins [2]. The main protein involved in mitochondrial fission is dynamin-related protein 1 (Drp1). During fission, Drp1 is recruited in the mitochondrial outer membrane by several mitochondria-bound proteins, including mitochondrial fission protein 1 (Fis1) and mitochondrial dynamics proteins (MiD49 and MiD51). At the fission sites, Drp1 forms ring-like structures that constrict the mitochondrial tubule to mediate fission. Meanwhile, mitochondrial fusion is regulated by mitofusin 1/2 (Mfn1/2) and optic atrophy 1 (Opa1). Mfn1/2 and Opa1 are located in the outer and inner mitochondrial membrane, respectively, and promote mitochondrial membrane fusion.

Mitochondrial dynamics are essential in maintaining cellular and mitochondrial functions. In the physiological state, mitochondrial fission equally divides the mitochondria into daughter cells in the late G2 and M phases and is also

associated with turnover of damaged mitochondria by autophagy. Regarding cellular energy metabolism, oxidative phosphorylation in fused mitochondria is known to be an activated status compared to that in fragmented mitochondria, suggesting a close relationship between mitochondrial morphology and cellular energy production. Additionally, a recent study showed that basal $[Ca^{2+}]i$ level and Ca^{2+} oscillation frequency decrease in Drp1 knockdown human hepatocellular carcinoma (HCC) BEL7402 cells, whereas an inverse response is observed in Drp1 overexpressed human HCC MHCC97L cells [3]. This result indicates that mitochondrial morphological status regulates cellular Ca^{2+} signaling, since Ca^{2+} is well accepted as important in maintaining cellular homeostasis, i.e., transcription factor activation, cell cycle regulation, and cellular transformation [4].

Several genotoxic agents (doxorubicin and cisplatin) [5-7] and oxidative stimulus (UV) [8] have been reported to facilitate mitochondrial fragmentation and release of reactive oxygen species (ROS) from mitochondria in tumor cell lines. In cardiac ischemia/reperfusion, mitochondrial fragmentation were also observed in the in vivo rat model [9]. In the elongated mitochondria-enriched status in Drp1-knockdown BEL7402 cells, the response of Ca^{2+} oscillation frequency to hydrogen peroxide treatment was reported to be smaller compared to that in wild-type BEL7402 cells [3].

These findings indicate that genotoxic and oxidative stimuli modulate various mitochondrial dynamics-related cellular functions. Our recent studies showed that ionizing radiation triggers mitochondrial fragmentation by promoting Drp1-dependent fission in mouse embryo fibroblasts (MEFs) and mouse fibroblasts, NIH3T3 cells [10-12]. Furthermore, it was demonstrated that ionizing radiation enhances mitochondria-derived ATP synthesis, ROS production, and mitochondrial respiration in NIH3T3 cells, HeLa cells, and human lung adenocarcinoma A549 cells [11,13,14]. Drp1 inhibition by a pharmacological inhibitor (mdivi-1) or genetic knockout (KO) attenuated not only the radiation-induced mitochondrial fragmentation but also radiation-induced clonogenic cell death and mitotic catastrophe, which is a type of cell death associated with aberrant mitosis [10], suggesting that radiation-induced mitochondrial fragmentation and its related function are, at least partially, related to radiation-induced cell death. However, the detailed mechanism of how mitochondrial fragmentation affects radiation-induced cell death is still unclear.

In the present study, to explore the mechanisms of radiation-induced cell death related to mitochondrial fragmentation, the involvement of cellular ATP synthesis, ROS production, and $[Ca^{2+}]i$ in mitotic catastrophe was investigated in mouse breast

cancer EMT cell lines stably expressing shRNA against mitochondrial fission proteins, Drp1 and Fis1.

2. MATERIALS AND METHODS

2.1. Reagents

The nuclear stain, DAPI and Annexin V, APC Ready Flow™ Reagent, and Trypan Blue Stain were obtained from Thermo Fisher Scientific (Waltham, MA, USA). The following antibodies were used: anti-Drp1 (BD Biosciences, Billerica, MA, USA), anti-Fis1 (GeneTex Inc., Irvine, CA, USA), anti-cleaved caspase-3 (Cell Signaling Technology, Beverly, MA, USA), anti-actin, and HRP-conjugated secondary antibodies (Santa Cruz Biotechnology, Santa Cruz, CA, USA). The Western Lightning Plus-ECL chemiluminescence detection kit was purchased from PerkinElmer (Waltham, MA, USA). Cell ATP assay reagent was obtained from Toyo Ink (Tokyo, Japan). CaSiR-1 AM was purchased from GORYO Chemical Inc. (Sapporo, Japan). N-acetylcysteine (NAC), 2-glucopyranoside ascorbic acid (AA-2G), and BAPTA-AM were obtained from Wako Pure Chemical Industries (Osaka, Japan).

2.2. Cell culture and X-irradiation

Murine breast cancer EMT6 cells were obtained from ATCC (CRL-2755) and maintained in RPMI1640 medium (Thermo Fisher Scientific) supplemented with 10% FBS (Biosera, Nuaille, France) at 37°C in a humidified atmosphere of 5% CO_2.

X-irradiation was performed using an X-Rad iR-225 (Precision X-Ray, North Branford, CT, USA) at 200 kVp, 15 mA, with a 1.0-mm aluminum filter.

2.3. Plasmids and stable transfection

XhoI site in the EF1-α promoter region of pEF6.mCherry-TSG101 (Addgene plasmid #38318) was destroyed by PCR-based site-directed mutagenesis. GFP-miR30 region from pENTR/pSM2(CMV) GFP (w513-1) (Addgene plasmid #19170) was then subcloned into the mutated pEF6.mCherry-TSG101 plasmid using BamHI and BstBI. The resultant plasmid that expresses GFP and miR30-based shRNA under the control of EF1-α promoter was named pEF6-GFP-miR30. Target sequences of shRNA against Drp1 and Fis1 were designed according to a previous study [15] and shown in Supplementary table 1. Moreover, 97-mer oligonucleotides coding for the respective shRNAs were PCR amplified using the primers 5´miR30-XhoI-fw and miR30-EcoOligo-rev as described [15]. After amplification, the fragments were excised using XhoI/EcoRI and cloned into pEF6-GFP-miR30. The sequences of all shRNA expression vectors were verified. The shRNA expression vectors were transfected into EMT6 cells using lipofection. Following blasticidin treatment (10 μg/mL), surviving clones with high GFP fluorescence were selected and maintained in RPMI1640/10%

FBS containing blasticidin (2.5 μg/mL). The knockdown efficiency was confirmed by Western blot analysis.

2.4. Mitochondrial morphology

Cells were seeded on 35-mm glass-bottomed dishes and cultured overnight. The cells were incubated in serum-free medium containing 100 nM MitoTracker Red for 30 min at 37°C. After washing with medium, fresh growth medium was supplied. Fluorescence images of live cells were obtained using an LSM700 confocal laser scanning microscope (Carl Zeiss, Oberkochen, Germany) at 37°C in 5% CO_2. To quantify mitochondrial morphology, mitochondrial shapes in the cell were categorized into "highly connected," "tubular," "intermediate," and "fragmented" as described in our previous study [12].

2.5. Western blot analysis

Cells were collected and lysed with lysis buffer. After centrifugation, supernatants were collected and added with 3× Laemmli sample buffer. Proteins were separated by SDS–PAGE and transferred into a nitrocellulose membrane (Advantec TOYO Inc, Tokyo, Japan). After blocking, the membrane was probed with specific antibodies

overnight at 4°C. After probing with HRP-conjugated secondary antibodies, the bound antibodies were detected with Western Lightning Plus-ECL. Image acquisition was performed with an LAS 4000 mini image analyzer (Fujifilm, Tokyo, Japan).

2.6. Clonogenic survival assay

After x-irradiation, cells were cultured for 6 days before methanol fixation and staining with Giemsa solution (Wako Pure Chemical Industries). Colonies containing >50 cells were scored as surviving cells. Surviving fractions were calculated, correcting for the plating efficiency of cells, with or without x-irradiation.

2.7. Trypan blue staining

After irradiation, cells were collected at indicated times. Following washing with PBS, the cells were stained with Trypan blue. Trypan blue positive cells were counted using Countess^{TM} II FL Automated Cell Counter (Thermo Fisher Scientific).

2.8. Apoptosis analysis

After irradiation, cells were collected at indicated times. For cleaved caspase-3 detection, the cells were fixed with ethanol. After centrifugation, the cells were

permeabilized and incubated with anti-cleaved caspase-3 antibody. After washing, the cells were incubated with the APC-conjugated anti-rabbit IgG. Flow cytometer analysis was conducted using the BD FACSVerse^{TM} Flow Cytometer (BD Biosciences), and the intensity of cleaved caspase-3 was measured. In Annexin V and PI staining, the cells were stained with Annexin V, APC Ready Flow^{TM} Reagent (Thermo Fisher Scientific), and PI for 15 min at room temperature. After staining, the cells were analyzed with flow cytometer.

2.9. Mitotic catastrophe analysis

Cells were seeded on glass coverslips and cultured overnight. After x-irradiation, cells were fixed using 3.7% paraformaldehyde/PBS for 10 min at 4°C and permeabilized with PBS containing 0.5% Triton X-100 for 5 min at 4°C, followed by DAPI staining. Coverslips were mounted with ProLong® Gold Antifade Mountant reagent (Thermo Fisher Scientific). Fluorescent microscopic analysis was performed using an Olympus BX61 microscope (Olympus, Tokyo, Japan) using reflected light fluorescence. At least 100 cells were analyzed. Where necessary, ROS scavengers (NAC and AA-2G) and intracellular Ca^{2+} chelator (BAPTA-AM) were used. After irradiation, the medium was

replaced with fresh growth medium containing drugs, and the cells were cultured for analysis.

2.10. Cellular ATP measurement

Total ATP was quantified using cell ATP assay reagent (Toyo Ink). The suspension of cells (1×10^5 cells) in a 96-well plate was mixed with luciferin-luciferase solution and incubated for 1 h at room temperature. Then, luminescence was measured using the Nivo multimode microplate reader (PerkinElmer).

2.11. Cellular Ca^{2+} measurement

After irradiation, cells were collected at indicated times. The cells were stained with 1 μM CaSiR-1-AM in HBSS for 1 h at 37°C. After staining, the cells were analyzed using a flow cytometer.

2.12. Statistical analysis

All results are expressed as means ± SD of at least three separate experiments. Comparison of the two groups was performed using Student's t-test. For multiple

comparisons, The Dunnett or Tukey-Kramer test was used. The minimum level of significance was set at a P-value < 0.05.

3. RESULTS

3.1. Effects of mitochondrial fission protein knockdown on mitochondrial morphologies

We initially established EMT6 cell lines stably expressing shRNA against mitochondrial fission proteins, Drp1 and Fis1 (shDrp1 and shFis1 cells). The expression levels of these proteins were confirmed by Western blot analysis (Fig. 1A). We then analyzed and categorized mitochondrial morphologies in these cells. As shown in Fig. 1B and 1C, Drp1 and Fis1 inhibition enhanced mitochondrial length and interconnectivity, suggesting that mitochondrial fission was successfully inhibited.

3.2. Effects of mitochondrial fission inhibition on radiosensitivity and radiation-induced cell death, necrosis, apoptosis, and mitotic catastrophe

To examine the effects of mitochondrial fission inhibition on cellular survival after x-irradiation, we performed clonogenic survival assay. X-irradiation decreased the viability of control cells in a dose-dependent manner. Drp1 and Fis1 inhibition reduced clonogenic cell death at a dose $\geq$ 2.5 Gy (Fig. 2A). In contrast, mitochondrial fusion inhibition by Mfn2 and Opa1 knockdown had no effects on cellular radiosensitivity, whereas mitochondrial shapes were drastically shortened (Supplemental Fig. 1). These

results indicate that inhibition of mitochondrial fission decreases cellular radiosensitivity.

It is known that ionizing radiation causes various types of cell death, including necrosis, apoptosis, mitotic catastrophe, and autophagy [16,17]. To investigate how downregulation of mitochondrial fission caused the reduction in radiosensitivity in EMT6 cells, we analyzed the modes of cell death after irradiation. First, we performed Trypan blue staining assay to evaluate membrane destructive cell death as necrosis. As shown in Fig. 2B, Trypan blue positive cells were < 10% 72 h after irradiation, and Drp1 and Fis1 inhibition did not affect it. Next, apoptotic cell death was analyzed by cleaved caspase-3 and Annexin V/PI staining. X-irradiation increased the expression of cleaved caspase-3 in a time-dependent manner (Fig. 2C) and induced early apoptosis (Annexin V positive and PI negative) to 10% (Fig. 2D). Drp1 knockdown partially decreased cleaved caspase-3 expression and early apoptosis at 72 h after irradiation, whereas Fis1 knockdown did not alter them. These results suggest that, although Drp1 seems to be slightly involved in apoptosis, apoptosis and necrosis are not major factors of radiation-induced cell death in EMT6 cells because irradiation of 5 Gy induced about half or more reduction in clonogenic survival. Mitotic catastrophe is a type of cell death associated with aberrant mitosis and considered a major cell death mechanism after

irradiation [16]. Then, we examined the effect of mitochondrial fission inhibition on mitotic catastrophe. After x-irradiation, we stained cell nuclei and scored the cells with features of aberrant mitotic nuclei, such as micronuclei, multilobular nuclei, and fragmented nuclei, as cells undergoing mitotic catastrophe (Fig. 2E). X-irradiation increased mitotic catastrophe to 60% in control cells (Fig. 2F, *white*). Downregulation of Drp1 and Fis1 significantly attenuated it to 30–40% (Fig. 2F, *black* and *gray*). This result suggests that mitotic catastrophe is a major factor of radiation-induced cell death in EMT6 cells and that mitochondrial fission is mainly involved in radiation-induced mitotic catastrophe.

3.3. Involvement of ATP production, ROS generation, and Ca^{2+} level in the induction of mitotic catastrophe after x-irradiation

To investigate how mitochondrial fission contributes to radiation-induced mitotic catastrophe, we analyzed the involvement of ATP production, ROS generation, and Ca^{2+} level. Regarding DNA damage and repair kinetics, there were no significant differences in shDrp1 and shFis1 cells (Supplemental Fig. 2). First, ATP production was analyzed. Although ATP production increased after irradiation, neither Drp1 nor Fis1 inhibition influenced it (Fig. 3). We examined the involvement of ROS in radiation-induced mitotic catastrophe using ROS scavengers, NAC, and AA-2G.

Neither NAC nor AA-2G influenced mitotic catastrophe after irradiation (Fig. 4A and 4B). Previous studies have suggested that the alteration in calcium homeostasis is closely associated with the status of mitochondrial fusion and fission [3,18]. Then, we confirmed the possibility that mitochondrial fission contributes to radiation-induced mitotic catastrophe via the regulation of cytosolic $[Ca^{2+}]i$ level. When cytosolic $[Ca^{2+}]i$ level was evaluated, it was slightly but significantly increased after irradiation at 12 h in control cells (Fig. 5A). In contrast, shDrp1 and shFis1 completely suppressed the increase in cytosolic $[Ca^{2+}]i$ level after irradiation. We further examined the effect of Ca^{2+} chelation on radiation-induced mitotic catastrophe, using BAPTA-AM. We confirmed that BAPTA-AM did not prevent cell cycle progression in EMT6 cells after irradiation. BAPTA-AM significantly reduced mitotic catastrophe after irradiation (Fig. 5B). These data suggest that cytosolic $[Ca^{2+}]i$ but not ATP and ROS production is involved in radiation-induced mitotic catastrophe and that mitochondrial fission is partially involved in mitotic catastrophe by increasing cytosolic $[Ca^{2+}]i$ level after irradiation.

4. Discussion

In the present study, we demonstrated that Drp1 and Fis1 knockdown reduced not only mitochondrial fission but also radiation-induced clonogenic cell death in EMT6 cells, (Fig. 1-2) as well as our previous data, using Drp1 KO MEFs [10]. These observations indicate that mitochondrial fission has an essential role in radiation-induced cell death induction. When the modes of cell death after irradiation were investigated, radiation-induced mitotic catastrophe was significantly reduced by mitochondrial fission inhibition (Fig. 2F). This result is well correlated with the clonogenic cell death. It is known that mitochondrial fission closely relates to apoptosis induction [2]. In fact, shDrp1 significantly but slightly decreased apoptosis after irradiation (Fig. 2D). However, since radiation-induced apoptosis was < 10%, its contribution to radio-protective effect by mitochondrial fission inhibition seems to be small in EMT6 cells. Taken together, these data suggest that inhibition of mitochondrial fission mainly decreased mitotic catastrophe but not necrosis and apoptosis after irradiation in EMT6 cells.

As shown in Fig. 5A, x-irradiation increased cellular $[Ca^{2+}]i$ level in EMT6 cells. Similarly, previous studies reported that ionizing radiation increases cytosolic $[Ca^{2+}]i$ level in several cell lines [19,20], indicating that this phenomenon is a universal reaction

in mammal cells. Our study also showed that this radiation-induced increase in cellular $[Ca^{2+}]i$ level was suppressed by mitochondrial fission inhibition. It is known that mitochondria serve as Ca^{2+} store to control intracellular Ca^{2+} signaling by buffering cytosolic $[Ca^{2+}]i$ [21]. Recently, it has been shown that inhibition of mitochondrial fusion increases store-operated Ca^{2+} entry in cardiomyocyte differentiation [22]. Moreover, Huang et al. have shown that mitochondrial fission increased cellular $[Ca^{2+}]i$ level by STIM1-mediated store-operated Ca^{2+} entry in HCC cells after hydrogen peroxide treatment [3]. These observations indicate that mitochondrial fission is involved in cellular $[Ca^{2+}]i$ regulation.

Furthermore, we demonstrated that intracellular Ca^{2+} was involved in radiation-induced mitotic catastrophe, while ATP synthesis and ROS production were not (Fig. 3-5) BAPTA-AM significantly decreased radiation-induced mitotic catastrophe (Fig. 5B). Ca^{2+} is known as a universal second messenger that regulates a number of diverse cellular processes, including execution of cell death [4]. Our previous study also showed that the increase in cellular $[Ca^{2+}]i$ level was triggered by irradiation and that BAPTA-AM delayed apoptosis induction in MOLT-4 cells [23]. Taken together, it is suggested that the regulation of cellular $[Ca^{2+}]i$ has an important role in cell survival after irradiation. However, how cellular Ca^{2+} contributes to mitotic

catastrophe remains unclear. Mitotic catastrophe is the major cell death mechanism after irradiation, and has been shown to occur as a premature reentry in mitosis with DNA damage [16]. In mitosis, various mitotic regulators, including cyclins, aurora kinases, and polo-like kinases, are strictly modulated by post-translational modification, synthesis, and degradation in a timely manner [24], and their improper regulation is involved in mitotic catastrophe. Aurora kinases play an essential role in mitosis by controlling centrosome segregation [25]. Recent study has reported that Ca^{2+} activates aurora A kinase in mitosis [26]. It also has been shown that cyclin B1 degradation is essential in metaphase–anaphase transition and mitotic exit, and its improper destruction in the M phase is associated with the execution of mitotic catastrophe [27]. Hyslop et al. reported that Ca^{2+} triggers cyclin B1 destruction during meiosis in mouse oocyte development [28]. In fact, our previous study showed that cyclin B1 degradation was prolonged after irradiation in Drp1 KO MEFs [10]. From these data, it is possible that the increase in cytosolic $[Ca^{2+}]i$ level is, at least, partially involved in defective mitosis by influencing the activity or expression of mitotic regulators, resulting in mitotic catastrophe after x-irradiation.

Therefore, the present study demonstrates that $[Ca^{2+}]i$ plays an important role in mitotic catastrophe induction and mitochondrial fission contributes to the increase in

$[Ca^{2+}]i$ level after irradiation, resulting in a part of radiation-induced mitotic catastrophe. These findings imply that the regulation of mitochondrial shape is involved in cellular survival via their functional alteration after irradiation. We believe that our findings contribute to the establishment of an approach to alter cellular radiosensitivity by interfering with mitochondrial dynamics.

Conflict of interest

The authors declare no conflict of interest.

Acknowledgements

This work was supported, in part, by Grant-in-Aids for Scientific Research from the Japan Society for the Promotion of Science [grant numbers 19J13470 (TB), 19J1150909 (KY), 19H04264, 19K22586 (HY), 17K10465 (TY), 18K19254 (OI)].

References

[1] S. Hoppins, L. Lackner, J. Nunnari, The machines that divide and fuse mitochondria, Annu Rev Biochem 76 (2007) 751-780.
[2] D.C. Chan, Fusion and fission: interlinked processes critical for mitochondrial health, Annu Rev Genet 46 (2012) 265-287.
[3] Q. Huang, H. Cao, L. Zhan, X. Sun, et al., Mitochondrial fission forms a positive feedback loop with cytosolic calcium signaling pathway to promote autophagy in hepatocellular carcinoma cells, Cancer Lett 403 (2017) 108-118.
[4] J. Humeau, J.M. Bravo-San Pedro, I. Vitale, et al., Calcium signaling and cell cycle: Progression or death, Cell Calcium 70 (2018) 3-15.
[5] S.A. Samant, H.J. Zhang, Z. Hong, et al., SIRT3 deacetylates and activates OPA1 to regulate mitochondrial dynamics during stress, Molecular and cellular biology 34 (2014) 807-819.
[6] C. Zhao, Z. Chen, J. Qi, et al., Drp1-dependent mitophagy protects against cisplatin-induced apoptosis of renal tubular epithelial cells by improving mitochondrial function, Oncotarget 8 (2017) 20988-21000.
[7] X.J. Han, Z.J. Yang, L.P. Jiang, et al., Mitochondrial dynamics regulates hypoxia-induced migration and antineoplastic activity of cisplatin in breast cancer cells, Int J Oncol 46 (2015) 691-700.
[8] Z. Zhang, L. Liu, S. Wu, et al., Drp1, Mff, Fis1, and MiD51 are coordinated to mediate mitochondrial fission during UV irradiation-induced apoptosis, FASEB J 30 (2016) 466-476.
[9] R. Zepeda, J. Kuzmicic, V. Parra, et al., Drp1 loss-of-function reduces cardiomyocyte oxygen dependence protecting the heart from ischemia-reperfusion injury, Journal of cardiovascular pharmacology 63 (2014) 477-487.
[10] T. Yamamori, S. Ike, T. Bo, et al., Inhibition of the mitochondrial fission protein dynamin-related protein 1 (Drp1) impairs mitochondrial fission and mitotic catastrophe after x-irradiation, Mol Biol Cell 26 (2015) 4607-4617.
[11] T. Yamamori, T. Sasagawa, O. Ichii, et al., Analysis of the mechanism of radiation-induced upregulation of mitochondrial abundance in mouse fibroblasts, J Radiat Res 58 (2017) 292-301.
[12] T. Bo, T. Yamamori, M. Suzuki et al., Calmodulin-dependent protein kinase II (CaMKII) mediates radiation-induced mitochondrial fission by

regulating the phosphorylation of dynamin-related protein 1 (Drp1) at serine 616, Biochem Biophys Res Commun 495 (2018) 1601-1607.
[13] T. Yamamori, H. Yasui, M. Yamazumi, et al., Ionizing radiation induces mitochondrial reactive oxygen species production accompanied by upregulation of mitochondrial electron transport chain function and mitochondrial content under control of the cell cycle checkpoint, Free Radic Biol Med 53 (2012) 260-270.
[14] H. Yasui, K. Yamamoto, M. Suzuki, et al., Lipophilic triphenylphosphonium derivatives enhance radiation-induced cell killing via inhibition of mitochondrial energy metabolism in tumor cells, Cancer Lett 390 (2017) 160-167.
[15] C. Fellmann, T. Hoffmann, V. Sridhar, et al., An optimized microRNA backbone for effective single-copy RNAi, Cell Rep 5 (2013) 1704-1713.
[16] D. Eriksson, T. Stigbrand, Radiation-induced cell death mechanisms, Tumour Biol 31 (2010) 363-372.
[17] M. Chaurasia, A.N. Bhatt, A. Das et al., Radiation-induced autophagy: mechanisms and consequences, Free Radic Res 50 (2016) 273-290.
[18] G. Szabadkai, A.M. Simoni, K. Bianchi, et al., Mitochondrial dynamics and Ca2+ signaling, Biochim Biophys Acta 1763 (2006) 442-449.
[19] Y. Rai, R. Pathak, N. Kumari, et al., Mitochondrial biogenesis and metabolic hyperactivation limits the application of MTT assay in the estimation of radiation induced growth inhibition, Scientific reports 8 (2018) 1531.
[20] N. Heise, D. Palme, M. Misovic, et al., Non-selective cation channel-mediated Ca2+-entry and activation of Ca2+/calmodulin-dependent kinase II contribute to G2/M cell cycle arrest and survival of irradiated leukemia cells, Cellular physiology and biochemistry : international journal of experimental cellular physiology, biochemistry, and pharmacology 26 (2010) 597-608.
[21] R. Rizzuto, D. De Stefani, A. Raffaello, et al., Mitochondria as sensors and regulators of calcium signalling, Nat Rev Mol Cell Biol 13 (2012) 566-578.
[22] A. Kasahara, S. Cipolat, Y. Chen, et al., Mitochondrial fusion directs cardiomyocyte differentiation via calcineurin and Notch signaling, Science 342 (2013) 734-737.
[23] K. Takahashi, O. Inanami, M. Kuwabara, Effects of intracellular

calcium chelator BAPTA-AM on radiation-induced apoptosis regulated by activation of SAPK/JNK and caspase-3 in MOLT-4 cells, International journal of radiation biology 75 (1999) 1099-1105.
[24] T. Hunt, The requirements for protein synthesis and degradation, and the control of destruction of cyclins A and B in the meiotic and mitotic cell cycles of the clam embryo, The Journal of Cell Biology 116 (1992) 707-724.
[25] E.A. Nigg, Mitotic kinases as regulators of cell division and its checkpoints, Nat Rev Mol Cell Biol 2 (2001) 21-32.
[26] O.V. Plotnikova, E.N. Pugacheva, R.L. Dunbrack, et al., Rapid calcium-dependent activation of Aurora-A kinase, Nat Commun 1 (2010) 64.
[27] D.A. Brito, C.L. Rieder, Mitotic checkpoint slippage in humans occurs via cyclin B destruction in the presence of an active checkpoint, Curr Biol 16 (2006) 1194-1200.
[28] L.A. Hyslop, V.L. Nixon, M. Levasseur, et al., Ca2+-promoted cyclin B1 degradation in mouse oocytes requires the establishment of a metaphase arrest, Developmental Biology 269 (2004) 206-219.

Figure Legends

Fig. 1. Effect of protein knockdown involved in mitochondrial fission on mitochondrial morphologies

EMT6 cells stably expressing shRNA against proteins involved in mitochondrial fission were generated. (A) The expression levels of Drp1 and Fis1 in EMT6 cells stably expressing non-silencing shRNA (Ctl), shDrp1 or shFis1. (B and C) The cells were stained with MitoTracker Red, and mitochondrial morphologies were analyzed by confocal laser microscopy. (B) Representative images of mitochondria. (C) Quantitative analysis of mitochondrial morphologies.

Fig. 2. Effects of mitochondrial fission inhibition on clonogenic cell death, necrosis, apoptosis, and mitotic catastrophe after x-irradiation

(A) The effects of mitochondrial fission inhibition on survival fraction after x-irradiation. Data are expressed as means ± SD of the three experiments. *$p < 0.05$ vs. Ctl (Student's t-test). (B-D) After x-irradiation at 10 Gy, cells were cultured for the indicated times, and necrotic and apoptotic cell deaths were evaluated. (B) Trypan blue positive cells were counted. (C) The intensity of cleaved caspase-3 was measured. (D)

Cells in the early apoptosis (Annexin V positive, PI negative) were counted. (E and F) After the cells were x-irradiated at 5 Gy and incubated for 24 h, cell nuclei were stained with DAPI. (E) Representative images of the cells possessing features of mitotic catastrophe, such as micronuclei, multilobular nuclei, and fragmented nuclei. (F) Quantitative analysis of the effects of mitochondrial fission inhibition on radiation-induced mitotic catastrophe. Data are expressed as means ± SD of the three experiments. *$p < 0.05$ vs. Ctl (Dunnett test)

Fig. 3. Effect of mitochondrial fission inhibition on ATP production

(A) After x-irradiation at 10 Gy, cells were incubated for 24 h. The cells were collected, and cellular ATP was measured. Data are expressed as means ± SD of the three experiments. *$p < 0.05$ vs. 0 h (Dunnett test)

Fig. 4. Involvement of ROS production in the reduction in radiation-induced mitotic catastrophe by mitochondrial fission downregulation

After x-irradiation at 5 Gy, cells were incubated with or without NAC and AA-2G at indicated concentration for 24 h. (A) Quantitative analysis of the effects of NAC on radiation-induced mitotic catastrophe. (B) Quantitative analysis of the effects of AA-2G

on radiation-induced mitotic catastrophe. Data are expressed as means ± SD of the three experiments. *$p < 0.05$ vs. Ctl IR(+), DMSO (Dunnett test)

Fig. 5. Involvement of cellular Ca^{2+} in the reduction in radiation-induced mitotic catastrophe by mitochondrial fission downregulation

(A) The effects of mitochondrial fission inhibition on cellular [Ca^{2+}]i after irradiation. After x-irradiation at 5 Gy, cells were incubated for indicated times. The cells were collected and stained with CaSiR-1 AM and analyzed by flow cytometer. Data are expressed as means ± SD of the three experiments. *$p < 0.05$ vs. 0 h (Dunnett test). (B) Quantitative analysis of the effects of BAPTA-AM on radiation-induced mitotic catastrophe. After x-irradiation at 5 Gy, cells were incubated with or without 8 μM BAPTA-AM for 24 h. Data are expressed as means ± SD of the three experiments. *$p <$ 0.05 vs. Ctl IR(+), DMSO (Tukey-Kramer test)

Figure. 1
Click here to download high resolution image

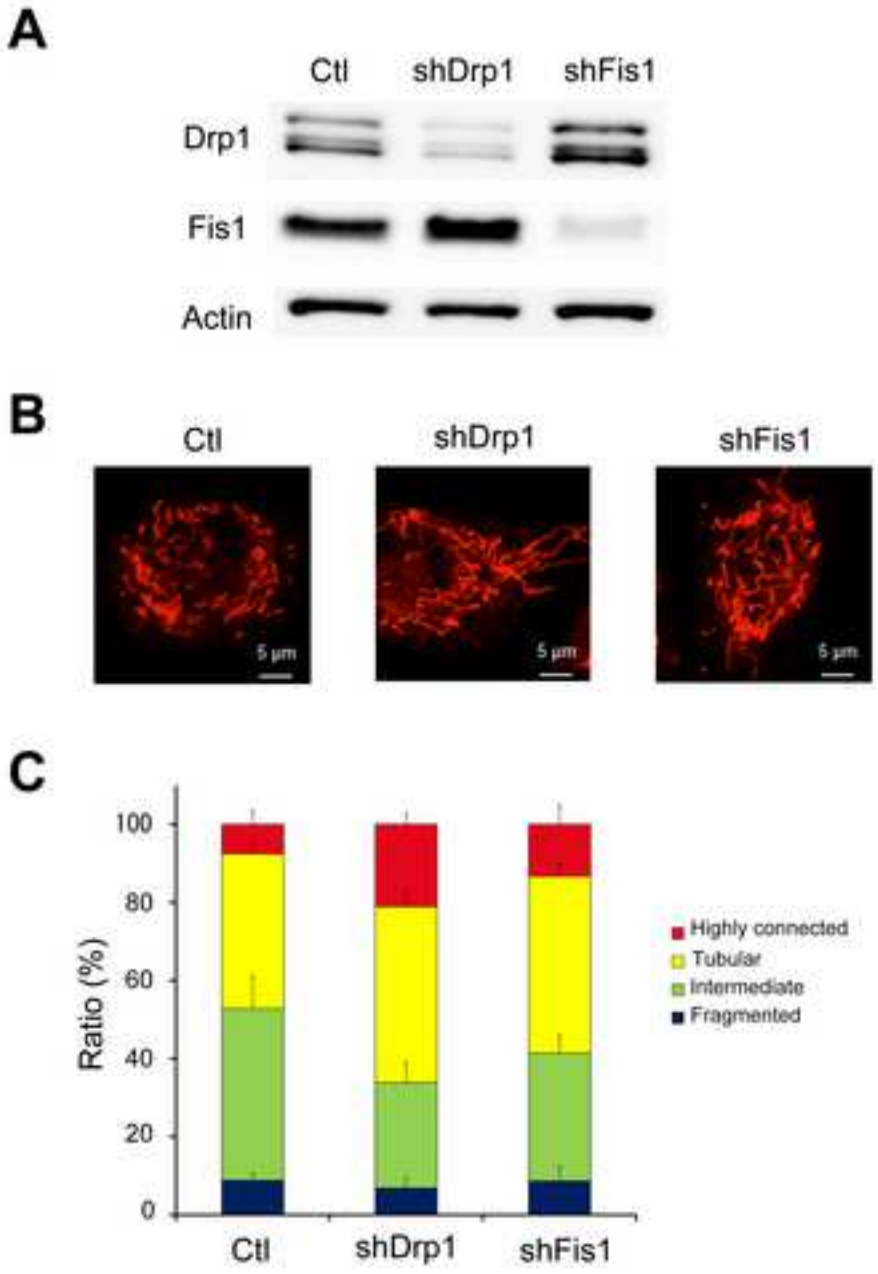

Fig.1 Bo et al.

Figure. 2

Click here to download high resolution image

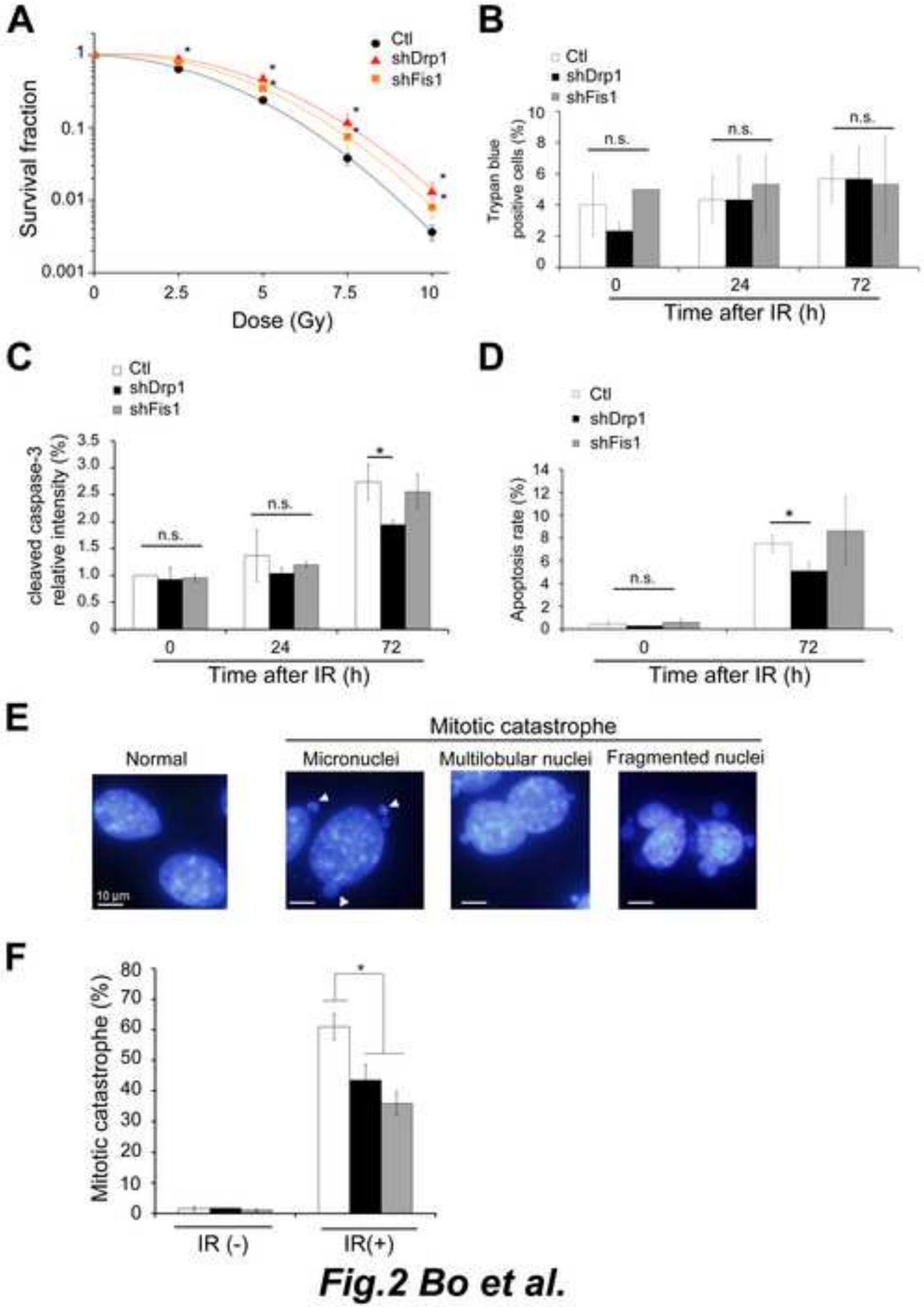

Fig.2 Bo et al.

Figure. 3
Click here to download high resolution image

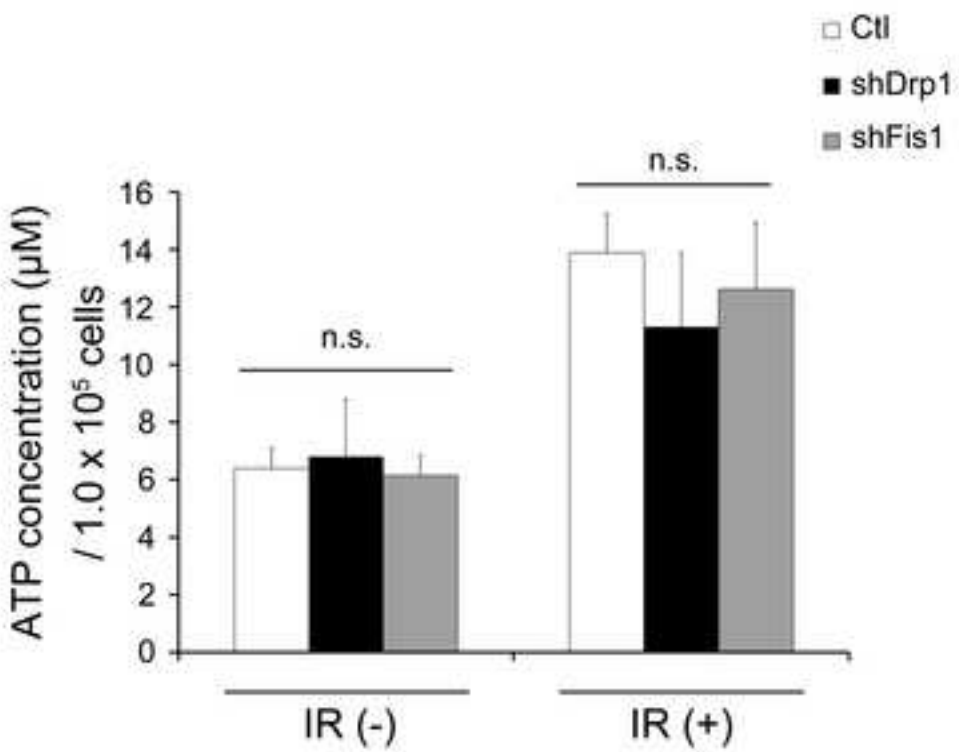

Fig.3 Bo et al.

Figure. 4
Click here to download high resolution image

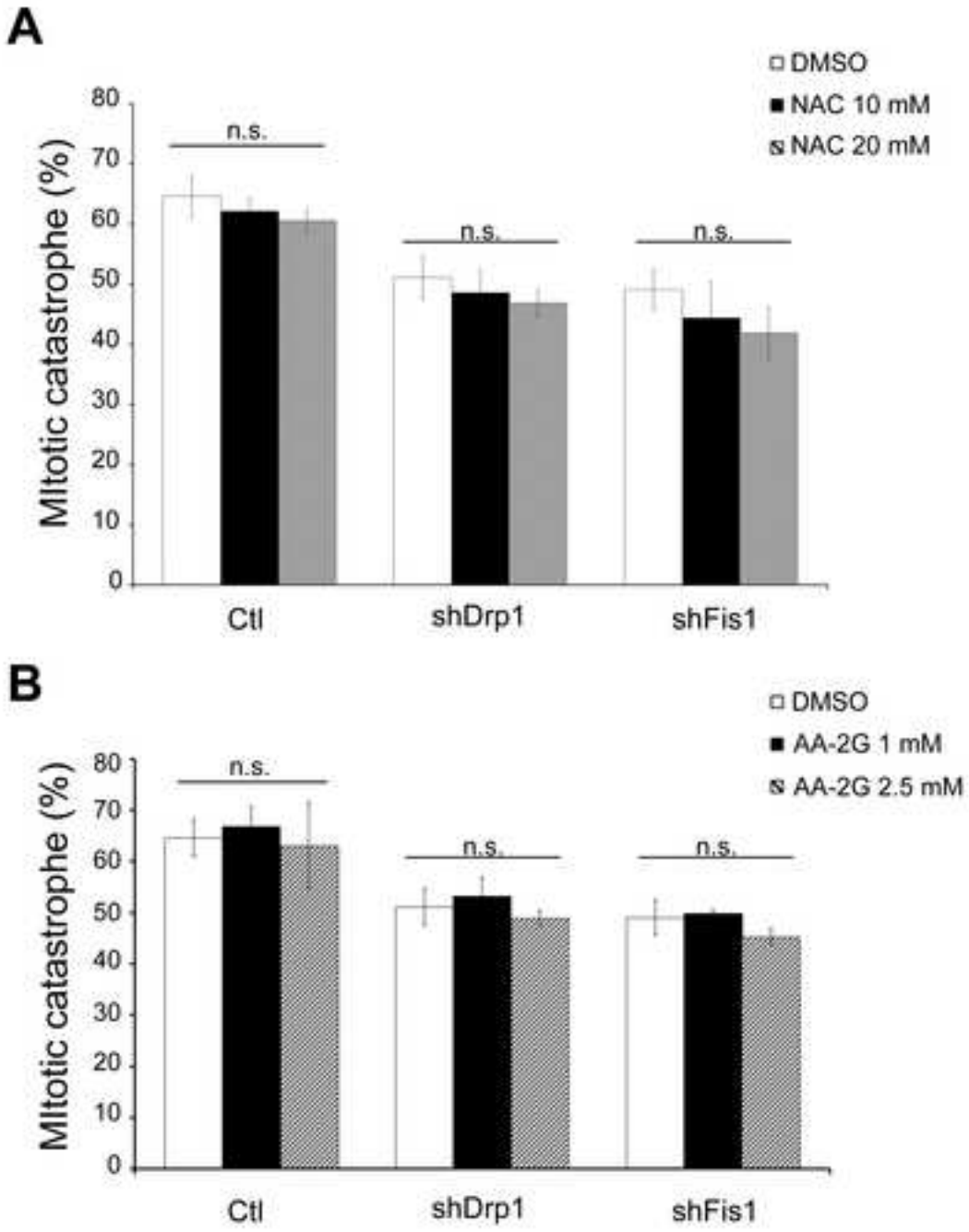

Fig.4 Bo et al.

Figure. 5
Click here to download high resolution image

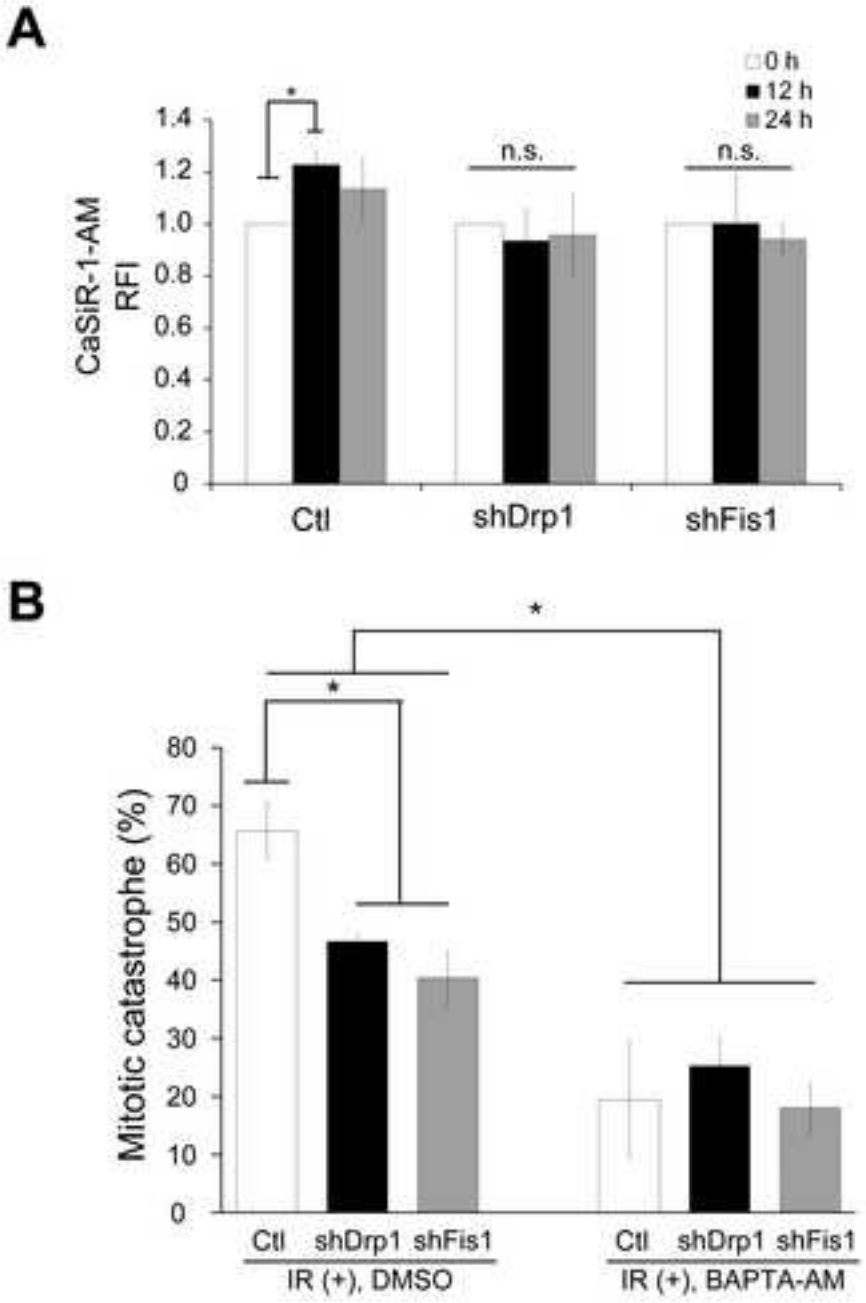

Fig.5 Bo et al.